Finite Difference Time Domain Simulation for the Brass Instrument Bore

Stefan Bilbao[a)]
Acoustics and Audio Group, King's Buildings, University of Edinburgh, Edinburgh, United Kingdom

John Chick
School of Engineering, King's Buildings, University of Edinburgh, Edinburgh, United Kingdom

(Dated: August 27, 2013)

In this article, interleaved finite difference time domain (FDTD) methods are developed for the purpose of simulating the dynamics of the acoustic bore, using, as a starting point, an impedance formulation of wave propagation in an acoustic tube; attention is focussed here on modeling of viscothermal and radiation losses in the time domain. In particular, in contrast to other methods, the bore, including the mouthpiece and bell, is treated as a unit, and is not subdivided into smaller units such as cylindrical or conical segments. Numerical simulations of input impedances are then compared with measurement for a variety of brass instruments.

PACS numbers: 4375Fg

I. INTRODUCTION

The wind instrument bore, among the systems of interest in musical acoustics, has seen a relatively large amount of scientific investigation; the modern line of research into acoustic tubes, and specialized to the case of wind instruments, goes back to the work of Benade[1] and others; for an overview of more recent developments, see, e.g., the review article by Campbell[2]. The starting point in many models of the dynamics of acoustic tubes is a 1D approximation, generally a variant of Webster's horn equation[3,4], suitable when wavelengths of interest are greater than the tube radius, which is approximately true for narrow bore members of the wind instrument family. Higher order effects may be modelled using multimodal approximations[5,6]. Though only brass instruments will be addressed in this article, it should be clear that all results are applicable to woodwind instruments as well.

From a simulation perspective, a variety of techniques are employed. As the bore is often characterised in terms of an impedance/admittance pair, frequency domain techniques have naturally long been applied for the analysis of both brass and woodwind instruments[7,8], and are often used to calculate the input impedance of the bore directly. A recent comparison of various models using frequency domain methods (the Transmission Line Matrix Method) is provided by Eveno et al.[9]. In sound synthesis applications for wind instruments, transmission line models (including methods employing wave variables such as digital waveguides[10–12] and other related methods[13]) are commonly used, as are modal methods[14].

Finite difference time domain (FDTD) methods, popularly used in electromagnetics simulation[15,16], are a good match to the simulation problem for an acoustic tube in 1D. The main distinctions between such techniques and other time domain methods (such as, e.g., digital waveguides) is that physical variables, such as pressure and velocity are employed rather than wave variables, and that the bore profile is treated as a unit, rather than discretized into sections of simpler form (such as, e.g., cylinders or cones). Though efficient solutions are ruled out by such an approach in the cases of simplified geometries such as the pure cylinder or cone[12,13], the approach allows for complete access to the internal state of the bore, and is thus more flexibly generalized—some such generalizations will be discussed in the conclusion of this article. 1D FDTD methods for brass instrument synthesis have been discussed previously by one of the present authors[17,18], and in 2D by Noreland[19].

A 1D PDE system for the acoustic tube, including radiation effects, and based on an impedance formulation is described in Section II; various approximations are then compared, especially with regard to accurate modeling of viscothermal losses. FDTD methods are introduced in Section III, with special attention paid to modeling methods for such losses. The accurate determination of bore profiles and input impedances for three representative brass instruments, including the mouthpiece, is discussed in Section IV. Finally, in Section V, simulation results, and a comparison against measurement is presented.

II. BORE MODEL

A. Impedance Formulation

The standard starting point in linear models of wave propagation in tubes including viscothermal effects is an impedance formulation. Following Benade[20] and earlier work[21,22], for the case of a uniform cylindrical tube of length L m, the pressure $\hat{p}(z,\omega)$ and particle velocity $\hat{v}(z,\omega)$, both functions of axial coordinate z along the tube and with harmonic time dependence $e^{j\omega t}$, for fre-

a)Electronic address: sbilbao@staffmail.ed.ac.uk

quency ω, are related by

$$\frac{\partial \hat{p}}{\partial z} + Z\hat{v} = 0 \qquad \frac{\partial \hat{v}}{\partial z} + Y\hat{p} = 0 \tag{1}$$

for $z \in [0, L]$. $Z(\omega)$ and $Y(\omega)$ are given by

$$Z = \frac{j\omega Z_c}{c\left(1 - F_v\right)} \qquad Y = \frac{j\omega}{cZ_c}\left(1 + (\gamma - 1)\, F_t\right) \tag{2}$$

Here, c is the wave speed, $Z_c = \rho c$ is the characteristic impedance, where ρ is air density, and γ is the ideal gas constant in air. The functions F_v and F_t are defined by

$$F_v = \phi(\sqrt{-j}r_v) \quad F_t = \phi(\sqrt{-j}r_t) \quad \phi(\xi) = \frac{2}{\xi}\frac{J_1(\xi)}{J_0(\xi)}$$

where J_0 and J_1 are Bessel functions of zeroth and first order, respectively, and where the nondimensional quantities r_v and r_t are given by

$$r_v = a\sqrt{\frac{\rho\omega}{\eta}} \qquad r_t = \nu a\sqrt{\frac{\rho\omega}{\eta}} \tag{3}$$

in terms of the frequency ω, density ρ, tube radius a, Prandtl number ν^2 and shear viscosity coefficient η.

System (1) can be reduced to a single equation in p, as

$$\frac{\partial^2 \hat{p}}{\partial z^2} = \Gamma^2 \hat{p} \qquad \Gamma = (ZY)^{1/2} \tag{4}$$

Values for the various constants used in this section, including temperature dependence, appear in Appendix A.

B. Approximations

Simple approximations are given by Keefe[23], valid in the ranges $r_v, r_t > 1$ and $r_v, r_t < 1$. For typical brass instrument geometries, the frequency at which the transition between the two ranges occurs is exceedingly small, and thus it is the former approximation which is of interest. For example, for a tube of radius 1 mm (which is perhaps the smallest imaginable occurring in a brass instrument, in the "throat" section of the bore), and at room temperature, the transition occurs at approximately 2.5 Hz.

The large r approximation may be written as

Model A:

$$Z_{(A)} = \rho\omega\left(j + \frac{2j^{1/2}}{r_v} + \frac{3}{r_v^2} + \left(\frac{15\sqrt{2}}{8} - \frac{j}{\sqrt{2}}\right)\frac{1}{r_v^3}\right) \tag{5a}$$

$$Y_{(A)} = \frac{\omega}{\rho c^2}\left(j + (\gamma - 1)\left(\frac{2j^{1/2}}{r_t} - \frac{1}{r_t^2} + \frac{j^{3/2}}{4r_t^3}\right)\right) \tag{5b}$$

The first terms in each approximation correspond, in isolation, to lossless wave propagation.

In the interest of simplification, the following approximation may also be considered:

Model B:

$$Z_{(B)} = \rho\omega\left(j + \frac{2j^{1/2}}{r_v} + \frac{3}{r_v^2}\right)$$

$$Y_{(B)} = \frac{\omega}{\rho c^2}\left(j + \frac{2\left(\gamma - 1\right)j^{1/2}}{r_t}\right)$$

The approximation above differs considerably from that given by Caussé, Kergomard and Lurton[8]. Approximate forms for Γ may be defined, for each of the above approximations, by $\Gamma^2_{(A)} = Z_{(A)}Y_{(A)}$ and $\Gamma^2_{(B)} = Z_{(B)}Y_{(B)}$.

Note that the terms in $Z_{(B)}$ and $Y_{(B)}$ Model B above have not been truncated to the same order; in particular, the term $-\frac{\omega(\gamma-1)}{\rho c^2 r_t^2}$ in $Y_{(A)}$ has been dropped. The reason is that when truncated to this order, the admittance is not positive real, and in fact approaches a negative value in the limit of low frequencies. While this is not problematic in frequency domain approaches, in time domain methods, such a term corresponds to non-passive behaviour; while such active behaviour may indeed be compensated for in the entire system by losses in the impedance, numerical design is considerably complicated in this case. In general, truncation of series representations of impedances is a major concern in time domain numerical design.

In some numerical approaches (and in particular those based on the use of digital waveguides[24]), a second order equation of the form (4) is modelled directly. In this case, a further simplification involves an approximation directly to $\Gamma^2 = ZY$, obtained from the product of $Z_{(B)}$ and $Y_{(B)}$ above, and retaining terms of order r_v^{-1} and r_t^{-1}:

Model C:

$$\Gamma^2_{(C)} = \frac{-\omega^2}{c^2}\left(1 - 2j^{3/2}\left(\frac{1}{r_v} + \frac{(\gamma - 1)}{r_t}\right)\right)$$

In the present case of a cylindrical tube, this approximation is identical, when used in the second order equation (4), and transformed to the time domain, to the Webster Lokshin formulation, used extensively recently in transmission line modeling of acoustic tubes[25], and also brass instruments[12,24].

It is useful to compare the approximations above in terms of loss α and phase velocity v_p, where

$$\Gamma_{(\cdot)} = \alpha + j\omega/v_p$$

See Figure 1, showing percentage errors for α and v_p for the three models A, B, and C, relative to (2) in the case of a very thin tube of radius 1 mm (a worst case, for brass instruments), over the range of frequencies between 1 Hz and 1000 Hz. Note that approximations (A) and (B) above give acceptable results for frequencies above about 20 Hz, whereas approximation (C) is noticeably poorer, especially in terms of loss, which is greatly underapproximated. (The approximation given by Benade[20] is of a similar character, though it gives a slightly better match than model C.) For wider tubes, however, the differences among the approximations quickly become less significant.

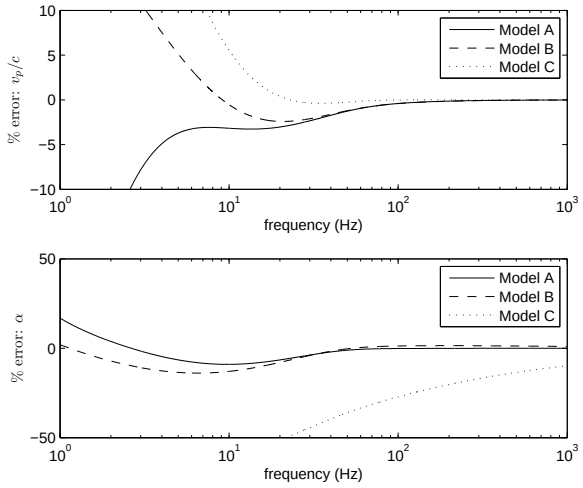

FIG. 1. Percentage error in relative phase velocity v_p/c (top) and loss α (bottom) for the models A, B, and C, relative to the expression in (2), as a function of frequency in Hz. Here, temperature is taken to be 26.85° C, and the tube is of radius 1 mm.

Given these results, and also that approximation (A) cannot be resolved in terms of factors of $j\omega$ alone, necessary in representing the system in the time domain in terms of time differential operators, approximation (B) will be used henceforth here.

C. Variable Geometry and Spatiotemporal Formulation

When wavefronts are assumed to be planar, system (1) can be extended to the case of variable horn geometry as

$$\frac{\partial p}{\partial z} + Zv = 0 \qquad \frac{\partial (Sv)}{\partial z} + SYp = 0 \tag{7}$$

where $S(z) = \pi a^2$ is the horn cross-sectional area at coordinate z.

Under the approximation of Z and Y by $Z_{(B)}$ and $Y_{(B)}$ above, and under the transformation to the time domain, (7) may be written as

$$\rho\partial_t v + \partial_z p + qv + f\partial_{t^{1/2}} v = 0 \tag{8a}$$

$$\frac{S}{\rho c^2}\partial_t p + \partial_z (Sv) + g\partial_{t^{1/2}} p = 0 \tag{8b}$$

where $p = p(z,t)$ and $v = v(z,t)$ are the pressure and particle velocity in the horn and where ∂_t and ∂_z represent partial differentiation with respect to t and z, respectively. $\partial_{t^{1/2}}$ represents a fractional derivative in time of order 1/2. The functions $f(z)$ $q(z)$ and $g(z)$ are given by

$$f = \frac{2\rho^{1/2}\eta^{1/2}}{a} \qquad q = \frac{3\eta}{a^2} \qquad g = \frac{2(\gamma-1)\eta^{1/2}\pi a}{\nu c^2 \rho^{3/2}}$$

System (8) above reduces to the well-known Webster horn equation under lossless conditions, and assuming plane wave propagation; similar forms may be written in terms of a single coordinate, for spherical and other wavefront types[26]; such generalizations are easy to incorporate into the present setting of FDTD design. Because the focus here is on the exposition of the issues involved in the use of FDTD methods, rather than on inter-model comparisons, the simplest model has been chosen, and generalizations as mentioned above will not be discussed further here.

D. Boundary Conditions

A single boundary condition must be supplied at each end of the domain $z \in [0, L]$ over which the bore is defined. In the case of brass instruments, $z = 0$ is taken to refer to the mouthpiece, and $z = L$ to the bell termination.

In the present case of a study of calculated input impedance, it is convenient to specify an impulsive volume velocity $u_0(t) = \delta(t)$, from which the boundary condition $v(0,t) = u_0(t)/S(0)$ follows.

At the radiating end of the bore, as in previous studies[8,9], approximations to the radiation impedance formula due to Levine and Schwinger[27] in the case of an unflanged circular pipe will be employed here. It is important, in FDTD simulations (as opposed to the case, in, e.g., frequency domain methods) that the approximation to the impedance is positive real, and thus passive.

There are various such positive real approximations available, and to illustrate passivity, and for ease of implementation, it is useful to represent them in terms of a concrete circuit representation, composed of inductors, capacitors and resistors, where pressures are interpreted as voltages, and velocities as currents. For concrete passivity, all element values must be non-negative. One arrangement, corresponding to an approximation given by Silva et al.[28], is as shown in Figure 2.

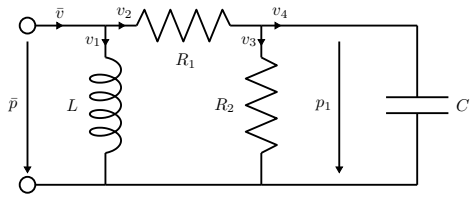

FIG. 2. Circuit representation of a radiation impedance boundary condition.

The one-port is defined by its terminal voltage/current pair, which are simply pressure $\bar{p} = p(L,t)$ and velocity $\bar{v} = v(L,t)$ at the right end of the bore. The corresponding loop and node equations, written in terms of internal state variables p_1 and v_1 ,v_2, v_3 and v_4, as indicated in

Figure 2, are as follows:

$$\bar{v} = v_1 + v_2 \qquad \bar{p} = L dv_1/dt \qquad \bar{p} = R_1 v_2 + p_1 \tag{9}$$

$$v_2 = v_3 + v_4 \qquad p_1 = R_2 v_3 \qquad v_4 = C dp_1/dt \tag{10}$$

Appropriate settings for the circuit element values may be derived[28] as

$$R_1 = \rho c \quad L = 0.613\rho a \quad R_2 = 0.505\rho c \quad C = 1.111\frac{a}{\rho c^2}$$

The resulting impedance Z_{rad} may be written in terms of factors of $j\omega$, as

$$Z_{rad} = \frac{L\left(R_1 + R_2\right) j\omega + LR_1R_2C\left(j\omega\right)^2}{R_1 + R_2 + \left(L + R_1R_2C\right) j\omega + LR_2C\left(j\omega\right)^2} \tag{11}$$

which is often examined in terms of the reflectance $\mathcal{R}$, defined by

$$\mathcal{R} = \frac{\rho c - Z_{rad}}{\rho c + Z_{rad}} = |\mathcal{R}| e^{2j(\omega a/c)(l/a)}$$

See Figure 3, showing a comparison between reflectance magnitude $|\mathcal{R}|$ and dimensionless length correction l/a for the Levine and Schwinger model and the impedance given in (11).

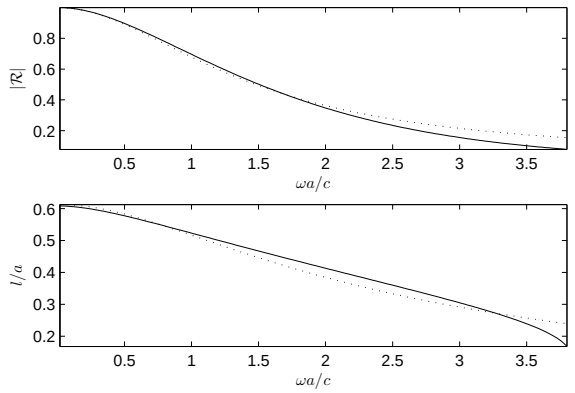

FIG. 3. Reflectance magnitude (top) and dimensionless length correction (bottom) for an unflanged cylindrical tube; the model given by Levine and Schwinger[27] is plotted as a solid line, and that of the approximation given in Silva et al.[28] as a dotted line.

The approximation given above is a good match to instruments without too wide a flare of the bore, over the typical playing range of a brass instrument; for better accuracy, one could attempt to fit higher order positive real impedances to the Levine and Schwinger model—this however, is a rather involved undertaking in general, as simple two-element structures such as Foster or Cauer networks are not sufficient to represent such an impedance—more general network synthesis procedures such as that of Brune[29] may be useful here, provided that a means of optimizing over such structures is available. More refined radiation models taking effects of curvature in non-cylindrical horns into account are available[30,31]; in such cases, care must be taken to ensure that the impedance remains positive real.

III. FINITE DIFFERENCE TIME DOMAIN METHOD

Finite difference time domain methods have been applied across a wide variety of disciplines, and especially electromagnetics[15,16], and geophysics[32], and are also an excellent match to problems in acoustics. In the present case of the acoustic tube, however, the situation is complicated somewhat by the appearance of fractional derivatives in the model system, requiring some care at the design stage.

A. Interleaved Grids and Difference Operators

A time domain simulation normally operates with a given fixed time step $k = 1/F_s$, where F_s is a sample rate. In simulations of musical instruments, the sample rate must normally be chosen greater than approximately 40 kHz.

As in electromagnetics FDTD applications[16], the relatively symmetric form of the system (8) in v and p suggests the use of an interleaved grid. Let p_l^n represent an approximation to $p(z,t)$ at $z = lh$, and $t = nk$, for integer $n \geq 0$, and $0 \leq l \leq N$; here $h = L/N$ for a given bore length L is the spacing between adjacent values of p_l^n. Similarly, let $v_{l+1/2}^{n+1/2}$ represent an approximation to $v(x,t)$, at $z = (l+1/2)h$, and $t = (n+1/2)k$, for integer $n \geq 0$ and $0 \leq l \leq N-1$. See Figure 4, illustrating the arrangement of grid values.

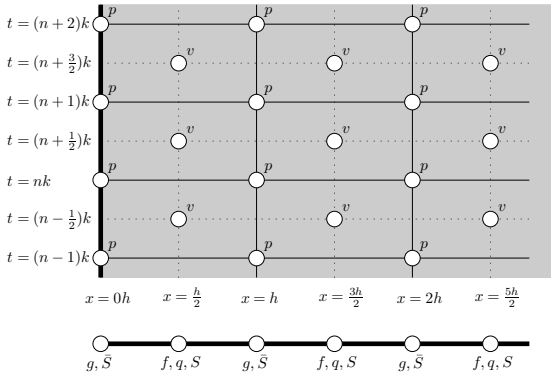

FIG. 4. Illustration of the interleaved arrangement of grid values for v and p, and locations at which the discrete functions f, q, g, S and $\bar{S}$ must be specified; the latter two quantities are approximations to $S(x)$, and are discussed in Section III.B.

For compactiness of notation, it is useful to introduce various difference and averaging operators. For a given grid function g_l^n, for integer or half-integer l and n, e_{t+} and e_{t-} represent forwards and backwards time shifts, and are defined as

$$e_{t+}g_l^n = g_l^{n+1} \qquad e_{t-}g_l^n = g_l^{n-1}$$

Similarly, spatial shifts e_{z+} and e_{z-} are defined as

$$e_{z+}g_l^n = g_{l+1}^n \qquad e_{z-}g_l^n = g_{l-1}^n$$

Forward and backward difference operators in time, δ_{t+} and δ_{t-}, and space, δ_{z+} and δ_{z-} may be defined in terms of the unit shifts as

$$\delta_{t+} = \frac{1}{k}\left(e_{t+} - 1\right) \qquad \delta_{t-} = \frac{1}{k}\left(1 - e_{t-}\right) \tag{12a}$$

$$\delta_{z+} = \frac{1}{h}\left(e_{z+} - 1\right) \qquad \delta_{z-} = \frac{1}{h}\left(1 - e_{z-}\right) \tag{12b}$$

Also useful are averaging operations μ_{t+} and μ_{t-}, defined as

$$\mu_{t+} = \frac{1}{2}\left(e_{t+} + 1\right) \qquad \mu_{t-} = \frac{1}{2}\left(1 + e_{t-}\right) \tag{13}$$

B. Scheme

An interleaved scheme for system (8) may be written, in operator form by employing the difference and averaging operators given in (12) and (13), as

$$\rho\delta_{t-}v + \delta_{z+}p + q\mu_{t-}v + f\delta_{t^{1/2}}\mu_{t-}v = 0 \tag{14a}$$

$$\frac{\bar{S}}{\rho c^2}\delta_{t+}p + \delta_{z-}\left(Sv\right) + g\delta_{t^{1/2}}\mu_{t+}p = 0 \tag{14b}$$

Here, grid indices have been suppressed; all instances of v and p refer to the grid functions p_l^n and $v_{l+1/2}^{n+1/2}$. Furthermore, the grid functions $q = q_{l+1/2}$, $f = f_{l+1/2}$ and $g = g_l$ are approximations to $q(z)$, $f(z)$ and $g(z)$ at the appropriate grid locations; $S_{l+1/2}$ and $\bar{S}_l$ represent distinct approximations to $S(z)$ at interleaved locations. The locations of these auxiliary functions on the spatial grid are indicated in Figure 4. In the present work, these values, have been drawn directly as samples through a spline-interpolated approximation to the measured bore profile, with the exception of S and $\bar{S}$, which are best chosen in a related manner—see below. Other possibilities, not explored here, might include integrating the bore profile over a grid spacing to obtain an averaged value at the grid locations, similarly to the procedure in finite volume methods[33].

The instances of the operator $\delta_{t^{1/2}}$ represent causal approximations to the fractional derivative operator, of which there are many varieties, and which are discussed in Section III.C. Notice also the use of averaging operators μ_{t+} and μ_{t-}, which serve to centre the action of the approximations to these fractional derivative.

Under the special choice of the interleaved approximations $S_{l+1/2}$ and $\bar{S}_l$ of

$$\bar{S}_l = \frac{1}{2}\left(S_{l+1/2} + S_{l-1/2}\right)$$

it is possible to show, under lossless conditions[34], that the scheme will be numerically stable under the Courant Friedrichs Lewy[35] condition

$$ck/h \leq 1 \tag{15}$$

regardless of the bore profile S. This implies, then, a minimal grid spacing h for a given time step k; in general, it is best to choose the grid spacing as close to this minimum value as possible, to minimize numerical dispersion. If $ck/h = 1$, the scheme (14) reduces to the well-known Kelly Lochbaum model used in acoustic tube modeling for speech synthesis[36].

C. Viscothermal Loss Approximations

Simple discrete approximations to the fractional derivative operator have been extensively investigated. A commonly used design is based on a discrete time approximation to the Grunwald-Leitnikow expansion, and takes the form:

$$\delta_{t^{1/2}} \Longrightarrow \frac{1}{\sqrt{k}}\sum_{r=0}^{M} c_r e_{t-}^r \tag{16}$$

The approximation is causal, as it depends only on powers of the backwards time shift operators e_{t-}, and may be interpreted as a finite impulse response (FIR) filter approximation of order M, where the coefficients c_r may be defined recursively as

$$c_0 = 1 \qquad c_r = \left(1 - \frac{3}{2r}\right)c_{r-1} \tag{17}$$

Low order recursive designs, based on the use of continued fraction expansions allow a much better match to the fraction derivative operation over nearly the entire frequency range of interest. A useful approximation makes use of an expansion of the Tustin transformation[37,38], or

$$\delta_{t^{1/2}} \Longrightarrow \sqrt{\frac{2}{k}}\left(\frac{1 - e_{t-}}{1 + e_{t-}}\right)^{1/2} \tag{18}$$

which, when the continued fraction expansion procedure is terminated after M steps, leads to an approximation of the form

$$\delta_{t^{1/2}} \Longrightarrow A^{-1}B \tag{19}$$

where

$$B = \sum_{r=0}^{M} b_r e_{t-}^r \qquad A = \sum_{r=0}^{M} a_r e_{t-}^r, \qquad a_0 = 1 \tag{20}$$

This approximation has the interpretation of a causal infinite impulse response (IIR) filter, of order M. Other IIR approximations, based on generalizations of the Tustin transformation are also available[39].

It is useful to compare the two designs in (16) and (19) at the same filter order M, in the present context of approximations to the behaviour of the brass instrument bore; note that for a given order M, and when employed in a scheme such as (14), both are on an equal footing in terms of memory requirements and the number of required arithmetic operations. To this end, consider the approximations in the frequency domain, where $\delta_{t^{1/2}}$ behaves as a multiplation by a factor $(j\omega)^{1/2}$, and the

approximations as multiplicative factors, where each instance of e_{t-} behaves as multiplication by $e^{-j\omega k}$. Figure 5 illustrates the behviour of the two approximations over the critical playing range of frequencies for brass instruments, between 0 and about 4000 Hz, when the sample rate F_s is chosen as 88 200 Hz. The response of the FIR approximation converges extremely slowly to that of the fractional derivative; indeed, even for a filter order of $M = 20$, the filter exhibits large inaccuracy over the normal playing range for a brass instrument. At an order of $M = 20$, the IIR approximation gives good results above approximately 100 Hz (inaccuracy below this frequency is easily observed in calculated inputed impedances—see Section V).

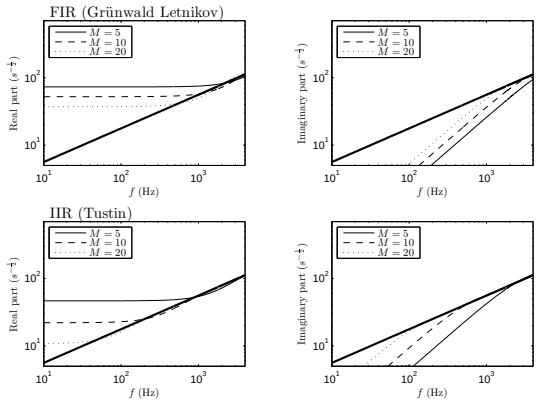

FIG. 5. Real and imaginary parts of approximations to the half derivative, in the frequency domain, at a sample rate of 88 200 Hz, for different orders of approximating filters, as indicated. Top: FIR approximation, and bottom, IIR approximation. The exact response of the half derivative is indicated by a thick black line.

D. Explicit Update Form

Under the approximation (19), which is causal, the scheme (14) may be written in an explicit update form, as

$$v = -\sum_{r=1}^{M} Q_{vv}^{(r)} e_{t-}^{r} v - \sum_{r=0}^{M} Q_{pv}^{(r)} e_{t-}^{r} p \tag{21a}$$

$$p = -\sum_{r=1}^{M} Q_{pp}^{(r)} e_{t-}^{r} p - \sum_{r=0}^{M} Q_{vp}^{(r)} e_{t-}^{r} v \tag{21b}$$

where the operators $Q_{vv}^{(r)}$, $Q_{pv}^{(r)}$, $Q_{pp}^{(r)}$ and $Q_{vp}^{(r)}$ are defined as

$$Q_{vv}^{(r)} = \frac{a_r - a_{r-1} + \frac{k}{2\rho}\left(q(a_r + a_{r-1}) + f(b_r + b_{r-1})\right)}{1 + \frac{k}{2\rho}\left(q + fb_0\right)}$$

$$Q_{pv}^{(r)} = \frac{k a_r \delta_{z-}}{\rho + \frac{k}{2}\left(q + fb_0\right)}$$

$$Q_{pp}^{(r)} = \frac{a_r - a_{r-1} + \frac{k\rho c^2}{2S} g(b_r + b_{r-1})}{1 + \frac{k\rho c^2}{2S} g b_0}$$

$$Q_{vp}^{(r)} = \frac{k\rho c^2 a_r \delta_{z+}\left(S\cdot\right)}{\bar{S} + \frac{k\rho c^2}{2} g b_0}$$

In a vectorized implementation, all the operators above may be represented as sparse matrix multiplications (where $Q_{vv}^{(r)}$ and $Q_{pp}^{(r)}$ in particular are diagonal).

The only remaining issue is the specialization of the operations at the boundary, which will be discussed in the next section.

E. Boundary Conditions

The scheme as presented in (14) necessarily requires boundary termination. In particular, the updates for pressure values p_0^{n+1} and p_N^{n+1} at locations $l = 0$ and $l = N$ respectively, according to (14b) require values of the velocity $v_{-1/2}^{n+1/2}$ and $v_{N+1/2}^{n+1/2}$, which lie outside the range of grid values over the interior. Update (14a), in contrast, does not require boundary termination.

The excitation to the system, for input impedance calculations, is an impulse in volume velocity $u_0 = u_0^n$, where $u_0^0 = 1$ and is zero otherwise. A suitable centred boundary termination for (14b) at location $l = 0$ is then

$$\frac{\bar{S}_0}{\rho c^2}\delta_{t-} p_0 + \frac{2}{h} u_0 + g A^{-1} B \mu_{t+} p_0 = 0 \tag{22}$$

For other types of excitation, and particularly if the bore is to be connected, e.g., to a lip model[18], then a more complex coupled condition between p_0^n and $v_{-1/2}^{n+1/2}$ must necessarily be resolved.

At the radiating end of the bore, an approximation to the impedance (11), or, equivalently, the system (9) must be employed. Here, it is the value $v_{N+1/2}^{n+1/2}$ which must be determined in order to complete the update of the pressure value p_N^n. To this end, set the values $\bar{p}^{n+1/2}$ and $\bar{v}^{n+1/2}$ as

$$\bar{p}^{n+1/2} = \mu_{t+} p_N^n$$

$$\bar{v}^{n+1/2} = \frac{1}{2\bar{S}_N}\left(S_{N-1/2} v_{N-1/2}^{n+1/2} + S_{N+1/2} v_{N+1/2}^{n+1/2}\right)$$

and the network definitions (9) may be employed, by substituting difference and averaging operators as necessary:

$$\bar{v}^{n+1/2} = \mu_{t+} v_1^n + \mu_{t+} v_2^n \qquad \bar{p}^{n+1/2} = L\delta_{t+} v_1^n$$

$$\bar{p}^{n+1/2} = R_1 \mu_{t+} v_2^n + \mu_{t+} p_1^n \qquad v_2^n = v_3^n + v_4^n$$

$$p_1^n = R_2 v_3^n \qquad \mu_{t+} v_4^n = C\delta_{t+} p_1^n$$

Here, the time series v_1^n, v_2^n, v_3^n v_4^n and p_1^n need not all be stored; the system above, when simplified and coupled with the scheme (14a) leads to an explicit update in p_N^n, p_1^n and v_1^n. Thus two extra units of storage are required to accommodate the reactive elements in the circuit representation of the impedance from Figure 2.

The discretization above essentially employs the trapezoid rule, and the termination becomes equivalent to a wave digital one port[40]; as such, there is some warping of the reflectance away from the approximated curves in Figure 3. For a sufficiently high sample rate, such warping effects will be very small over the playing range of the brass instrument (indeed, the approximation to the radiation impedance employed here is only valid over the range of frequencies with $\omega a/c \leq 3.8$).

IV. BORE AND INPUT IMPEDANCE MEASUREMENTS

The model was validated against three different types of orchestral brass instrument: trumpet, horn, and trombone. These instruments, shown in Figure 6, were selected to represent a broad range of bore profiles and playing ranges, and hence test the validity of the numerical method presented here. For each instrument, the bore profile was measured and used as an input to the model. The output from the model was then compared with acoustic impedance measurements taken from the same instruments. The details of each instrument are as follows:

FIG. 6. The instruments used for this study.

Trumpet The trumpet used was a Smith-Watkins B♭ trumpet with a Kelly 'Screamer' mouthpiece. This is a specialist high register combination with a very small mouthpiece cup volume. The overall length of the instrument, with no valves depressed, is approximately 1.38m, with a nominal pitch of $B\flat_2$

Trombone Conn 8H Artist Symphony tenor trombone in B♭ with a Denis Wick 5AL mouthpiece. This is a popular, professional level, orchestral trombone. Measurements were taken with the trombone slide in first position, giving an overall tube length of approximately 2.74m.

Horn This was a Meinl & Lauber/Paxman 'baroque' horn modelled after an eighteenth-century instrument by Huschauer, Vienna c.1770, together with a Paxman-Halstead-Chidell (PHC 22) mouthpiece. The instrument was crooked in D giving an overall tube length of approximately 4.51m, corresponding to a nominal pitch of D_1.

The bore profile was measured using techniques similar to those described by Myers[41]. The internal profile of the bell was determined using a series of graded rod gauges, attached to a rule allowing the insertion depth to be measured directly. For the smaller diameter sections, where access allowed, the bore was measured using internal dial calipers. For all other sections of the instrument, the external diameter was measured at regular intervals along the instrument with vernier calipers, and a nominal wall thickness deducted from this to arrive at a value for the bore. It is estimated that this procedure is accurate to within +/- 5%[41].

Axial measurements in bent sections were taken along the mid-line. It has recently been shown that the effect of a bend in the tubing of a wind instrument is frequency dependent and mostly, though not always, small[42]. For the trombone and horn, radii of curvature are large, and the effect is negligible; for the trumpet, even with no valves depressed, there will be higher curvature bends in the air column through the valve section, and this assumption is less justifiable, though it has still been taken here. A comparison of the bore profiles is shown in Figure 7.

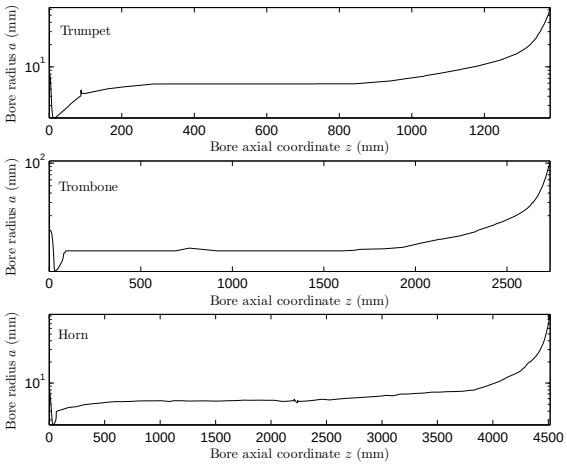

FIG. 7. Measured bore radius, vs. axial coordinate, in mm, with radius on a logarithmic scale for detail.

The input impedance for each of these instruments was measured using the commercially available BIAS system[43,44]. All impedance measurements were carried out in an anechoic room with temperatures controlled to

$19 - 20\,^{\circ}\mathrm{C}$. The experimental set up for the trombone is shown in Figure 8.

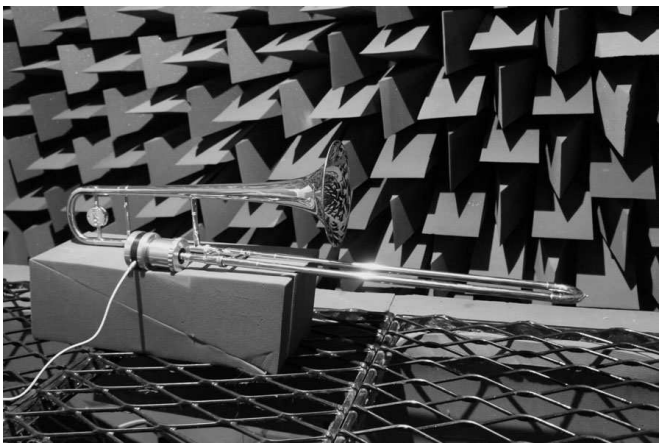

FIG. 8. Experimental set up for trombone input impedance measurements.

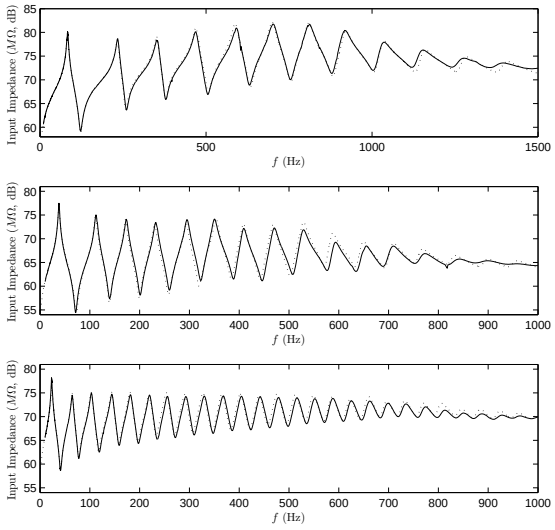

FIG. 9. Comparison between measured (solid line) and calculated (dotted line) input impedance magnitudes, in dB, for the three cases of the trumpet (top), trombone (middle) and horn (bottom). Here, the standard acoustic impedance (i.e. the ratio of pressure to volume velocity) has been plotted. In the finite difference scheme, volume velocity is determined from the calculated particle velocity by multiplication by $S(0)$.

V. SIMULATION RESULTS AND DISCUSSION

All simulation results in this section were produced using scheme (14), operating at 88.2 kHz. For a given bore length L, the grid spacing is chosen so as to evenly divide L, and satisfy the Courant condition (15) as closely as possible. The order of the Tustin approximation to the fractional derivative (see Section III.C) was chosen to be $M = 20$.

The input to the model was chosen as an impulsive volume velocity excitation, as described in Section III.E; the input impedance was taken as the unwindowed Fourier transform of the pressure time series p_0^n; the simulation duration was 10 s, or 882 000 samples in all cases.

Comparisons between calculated and measured input impedance magnitudes for the three instruments described in Section IV are shown in Figure 9; given that the curves are very closely matched, a standard algorithm searching for local extrema has been used, employing smoothing and parabolic fitting in the regions surrounding the peaks. The frequencies of the first seven maxima and minima of the input impedance curve for each instrument are given in Table I, along with percent difference in frequencies, as well as difference in magnitude, in dB. The frequencies match in most cases to under a percent, and amplitudes to within a dB or less; as such, these results are similar to those obtained using frequency domain methods such as the Transmission Line Matrix Method[9], in the present case of a simple plane wave model.

In the case of the trumpet and trombone, there is not a strong systematic bias in the frequencies or amplitudes of the extrema; in the case of the horn, however, such a bias is observable, with calculated frequencies slightly smaller than in the case of measurement, and amplitudes of extrema slightly higher; such a difference could well be attributed to inaccuracy in the temperature reading in this case.

More interesting is the inaccuracy in the first computed peaks, when these are at a particularly low frequency (as is the case for the trombone, and even more so for the horn). In this case, the inaccuracy is due to the viscothermal loss filter, which does not give a good approximation at such frequencies; this is a clear weakness of FDTD methods relative to purely frequency domain methods, which suffer no such inaccuracy (in theory, though similar problems have been noted in the case of the trombone using such methods[9]). To this end, it is interesting to compare calculated impedance curves in the low frequency region, in the worst case of the horn, under different orders M of the Tustin approximation to the fractional derivative. See Figure 10.

As a further comparison in this worst case of the lowest mode of the horn bore, the FDTD method described here was described with direct spatial integration of the frequency domain system (1), under the same approximations $Z_{(B)}$ and $Y_{(B)}$ to the impedance and admittance respectively, and using the same approximation to the radiation boundary condition (11). The system was integrated using a spatial step of 3.9 mm, and a frequency resolution of 0.3 Hz, and using a centred trapezoid rule scheme. As expected, above the extreme low frequency range (i.e., above about 50 Hz), the impedance curves calculated using FDTD and the frequency domain approach are virtually identical. In the case of the first mode of the horn, the frequency domain provides a better match, as illustrated in Figure 11.

The other well-known feature worth noting is the devi-

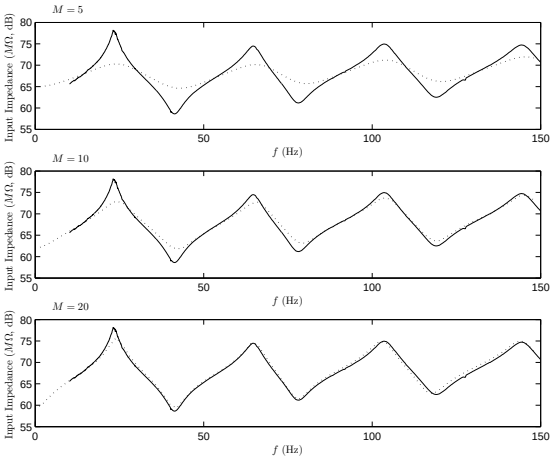

FIG. 10. Comparison between measured (solid line) and calculated (dotted line) input impedance magnitudes, in dB, for the horn, under different choices of the order M of the approximation to the fractional derivative operator. Top: $M = 5$, middle: $M = 10$ and bottom: $M = 20$.

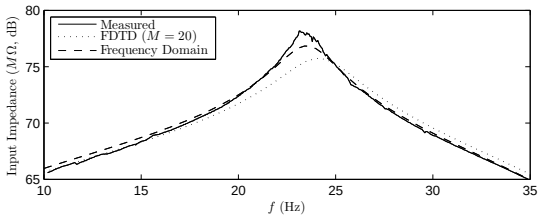

FIG. 11. Comparison between measured (solid line) FDTD at 88.2 kHz, with $M = 20$, (dotted line) and direct frequency domain integration (dashed line) input impedance magnitudes, in dB, for the horn, illustrating inaccuracy of the FDTD method relative to frequency domain calculation for the first mode of the horn.

ation of the calculated curves at higher frequencies, as is easily visible in Figure 9—a feature of 1D models which can be partly rectified using spherical (rather than planar) models of wave propagation, but can ultimately only be fully resolved using a multimodal approach.

VI. CONCLUSIONS AND FUTURE WORK

This article has been intended as an examination of construction techniques for finite difference time domain methods for the acoustic bore, and, through comparison with measured input impedance curves for a selection of brass instruments, as a validation of such methods.

At the level of the static linear bore model itself, various refinements are possible. The model presented here assumes simple planar wave propagation—various one-parameter generalizations of Webster's equation exist[26], including spherical wave propagation, which is well known to produce superior results[8,9]; such generalizations do not pose any major difficulties in the present

TABLE I. Measured and Calculated frequencies of the first seven maxima (+) and minima (−) of the input impedance magnitude for the three instruments, accompanied by percentage difference in frequencies, and amplitude difference in dB.

Trumpet, 20° C

Max/ Min	Measured Freq.(Hz)	Calculated Freq. (Hz)	% Diff.	Amplitude Diff. (dB)
(+)	83.5	83.0	-0.6	-0.1
(−)	122.5	122.6	0.1	-0.4
(+)	234.2	233.0	-0.5	-0.3
(−)	261.1	258.6	-1.0	0.1
(+)	353.1	351.5	-0.4	1.0
(−)	379.1	378.2	-0.2	0.2
(+)	469.1	469.7	0.1	0.8
(−)	505.6	507.3	0.3	0.3
(+)	591.6	588.3	-0.6	1.0
(−)	631.1	634.2	0.5	-0.4
(+)	702.7	699.6	-0.4	0.4
(−)	754.9	755.9	0.1	-0.4
(+)	812.5	809.8	-0.3	0.3
(−)	878.8	882.7	0.4	-0.6

Trombone, 19° C

Max/ Min	Measured Freq.(Hz)	Calculated Freq. (Hz)	% Diff.	Amplitude Diff. (dB)
(+)	38.3	38.2	-0.2	-0.9
(−)	71.8	73.2	2.0	-0.5
(+)	113.2	111.5	-1.5	-0.0
(−)	140.0	139.7	-0.2	-0.9
(+)	174.0	171.7	-1.3	-0.0
(−)	201.5	199.7	-0.9	-0.5
(+)	233.2	230.1	-1.3	-0.2
(−)	259.9	258.4	-0.6	-1.0
(+)	296.0	293.8	-0.8	-0.6
(−)	322.9	319.7	-1.0	-1.2
(+)	350.9	353.4	0.7	0.1
(−)	388.8	384.8	-1.0	-0.1
(+)	410.1	408.6	-0.4	1.0
(−)	446.4	442.6	-0.9	0.2

Horn, 20° C

Max/ Min	Measured Freq.(Hz)	Calculated Freq. (Hz)	% Diff.	Amplitude Diff. (dB)
(+)	23.2	24.1	3.8	-2.3
(−)	41.1	41.5	1.1	0.6
(+)	64.8	65.0	0.2	0.3
(−)	78.2	78.0	-0.1	0.1
(+)	103.7	102.9	-0.7	0.2
(−)	119.1	117.6	-1.2	0.1
(+)	144.7	144.1	-0.4	0.4
(−)	159.2	158.3	-0.6	0.4
(+)	181.9	180.7	-0.7	0.5
(−)	197.9	197.0	-0.5	0.3
(+)	220.3	219.1	-0.6	0.2
(−)	235.8	233.3	-1.1	0.7
(+)	256.2	253.8	-1.0	0.8
(−)	271.8	270.7	-0.4	0.4

context of FDTD methods. Models of viscothermal losses have been presented, to different degrees of approximation; some, such as model A, are not suitable for time domain discretization. Slight differences emerge under further approximation; in particular, model B appears to be a safe choice under virtually any realistic bore pro-

file. That being said, simulations using the simpler model C, for the realistic bore profiles presented here, led to deviations in the magnitudes of impedance maxima on the order of 0.2–0.3 dB from those calculated using model B.

At the level of numerical design, there are various features of interest.

Numerical stability for the algorithm as a whole, under the approximations to the fractional derivatives given in Section III.C remains unproven. That being said, numerical instability was not observed under any of the realistic test configurations examined here. An approach to the proof of numerical stability will necessarily involve showing first passivity of the approximation to the fractional derivative, which is possible through recourse to a decomposition of the continued fraction expansion of the Tustin operation into a passive RL network, under a continuous-to-discrete bilinear transformation, and furthermore to show conditions on ck/h, generalizing the condition (15), such that global passivity in ensured when such a network operates in conjunction with the bore itself. This second stage is less obvious, but it is conjectured here that the condition (15) will continue to hold under lossy conditions.

Another involves the approximation to the bore itself—the lower the sample rate, the larger the minimal grid spacing h becomes, from the stability condition (15). At a certain point, resolution of the fine features of the bore profile (particularly in the mouthpiece section) can be too crudely modeled, particularly if the cup volume is poorly approximated. An improvement is to be expected if methods employing variable grid spacings is employed, with little or no increase in computational cost—finite volume methods[33] are an excellent choice in this regard.

Finally, the modeling of viscothermal losses is something of a bottleneck in terms of memory requirements and operation count; though not extremely large in the case of standard instrument configurations, it is important to keep the filter order M as low as possible; $M = 20$ is sufficient for modeling virtually any brass instrument at a sample rate such as 88 200 Hz, with some inaccuracy in the lowest peak of the input impedance. Another approach to IIR design, rather than the use of the continued fraction expansion to the Tustin operator might be direct optimization of an IIR design, perhaps weighted towards good accuracy over the playing frequency range of the instrument.

One of the appealing features of such direct time domain methods is their extensibility and generality. Because of the very direct relationship between the numerical method and the underlying model problem, such extensions do not change the basic character of the method itself.

For example, the introduction of time varying components such as valves and slides into the method described here is direct, and thus could serve as a useful tool in the examination of transients under playing conditions; FDTD methods applied to a simple time-varying branched tube model of a valve has been presented recently[17]. One important point here is that when one of the branches is very severely constrained (e.g., when a valve is very slightly depressed), the approximation (5), and all of its descendants is no longer valid, and thus one may need to switch between large- and small-radius approximations during the course of a valved gesture. Another is that time variation, even if slow, as in the case of a brass instrument under playing conditions, must necessarily be viewed as a driving term—and thus care must be taken to ensure numerical stability, even under lossless conditions.

A more interesting extension is to the case of nonlinear wave propagation in the bore, which can lead to shock wave formation in long cylindrical bores (such as trombones), associated with an appreciable change in timbre at high playing amplitudes[45–47]. While it is possible to examine such nonlinear effects under some conditions at steady state using, e.g., frequency domain and harmonic balance techniques[48], an full examination of transients will ultimately require a time stepping technique of the type presented here. Finite volume methods[33] are an excellent choice in this regard, and, in 1D, not extremely different from the FDTD methods described here. Difficulties are to be expected, though, in the control of numerical oscillations during shock formation—while a large body of techniques for this purpose does exist, generally based on the use of artificial viscosity targeted at the region of shock formation[49], there is the danger that such losses will be so large as to distort the response of the instrument at high playing amplitudes.

TABLE II. Thermodynamic Constants

ρ	$1.1769(1 - 0.00335\Delta T)$ kg$\cdot$ m^{-3}
c	$3.4723\times10^{2}\,(1 + 0.00166\Delta T)\cdot$ s^{-1}m
η	$1.846\times10^{-5}\,(1 + 0.0025\Delta T)$ kg$\cdot$ s^{-1}m^{-1}
ν	$0.8410(1 - 0.0002\Delta T)$
γ	$1.4017(1 - 0.00002\Delta T)$

Acknowledgements

This work was supported by the European Research Council, under grant number StG-2011-279068-NESS. Thanks to the anonymous reviewers for their many valuable comments.

APPENDIX A: THERMODYNAMIC CONSTANTS

Values for the density ρ, wave speed c and gas constants η, ν and γ, as functions of temperature deviation ΔT from 26.85°C are given in Table II (as reproduced from Benade[20], and reprinted subsequently in Keefe[23]).

[1] A. Benade, "On woodwind instrument bores", Journal of the Acoustical Society of America **31**, 137–146 (1959).

[2] D. M. Campbell, "Brass instruments as we know them today", Acta Acustica united with Acustica **90**, 600–610 (2004).

[3] A. Webster, "Acoustical impedance, and the theory of horns and of the phonograph", Proceedings of the National

Academy of Sciences of the United States of America **5**, 275–282 (1919).

[4] S. Rienstra, "Webster's horn equation revisited", SIAM Journal of Applied Mathematics **65**, 1981–2004 (2005).

[5] A. Benade and E. Jansson, "On plane and spherical waves in horns with nonuniform flare I. Theory of radiation, resonance frequencies, and mode conversion", Acustica **31**, 79–98 (1974).

[6] V. Pagneux, N. Amir, and J. Kergomard, "A study of wave propagation in varying cross-section waveguides by modal decomposition. Part I. Theory and validation", Journal of the Acoustical Society of America **100**, 2034–2048 (1996).

[7] G. Plitnik and W. Strong, "Numerical method for calculating inputimpedance of the oboe", Journal of the Acoustical Society of America **65**, 816–825 (1979).

[8] R. Caussé, J. Kergomard, and X. Lurton, "Input impedance of brass musical instruments—comparison between experiment and numerical models", Journal of the Acoustical Society of America **75**, 241–254 (1984), Note: There is most likely a typographical error in the second expression for Y_t given on page 244 of this article.

[9] P. Eveno, J.-P. Dalmont, R. Caussé, and J. Gilbert, "Wave propagation and radiation in a horn: Comparisons between models and measurements", Acta Acustica United with Acustica **98**, 158–165 (2012).

[10] P. Cook, "Tbone: An interactive waveguide brass instrument synthesis workbench for the NeXT machine", in *Proceedings of the International Computer Music Conference*, 297–299 (Montreal, Canada) (1991).

[11] M. van Walstijn and D. Campbell, "Discrete-time modeling of woodwind instrument bores using wave variables", Journal of the Acoustical Society of America **113**, 575–585 (2003).

[12] R. Mignot, T. Hélie, and D. Matignon, "Digital waveguide modeling for wind instruments: Building a state space representation based on the Webster Lokshin model", IEEE Transactions on Audio, Speech, and Language Processing **18**, 843–854 (2010).

[13] P. Guillemain, J. Kergomard, and T. Voinier, "Real-time synthesis of clarinet-like instruments using digital impedance models", Journal of the Acoustical Society of America **118**, 483–494 (2005).

[14] C. Vergez, "Trompette et trompettiste: Un système dynamique non linéaire à analyser, modéliser et simuler dans un contexte musical", Ph.D. thesis, Université de Paris VI (2000), in French.

[15] K. Yee, "Numerical solution of initial boundary value problems involving Maxwell's equations in isotropic media", IEEE Transactions on Antennas and Propagation **14**, 302–307 (1966).

[16] A. Taflove, *Computational Electrodynamics*, 1–1038, third edition (Artech House, Boston, Massachusetts) (2005).

[17] S. Bilbao, "Modelling of brass instrument valves", in *Proceedings of the 14th International Digital Audio Effects Conference*, 337–344 (Paris, France) (2011).

[18] S. Bilbao, "Time domain simulation of brass instruments", in *Proceedings of Forum Acusticum* (Aalborg, Denmark) (2011).

[19] D. Noreland, "A numerical method for acoustic waves in horns", Acta Acustica united with Acustica **88**, 576–586 (2002).

[20] A. Benade, "On the propagation of sound waves in a cylindrical conduit", Journal of the Acoustical Society of America **44**, 616–623 (1968).

[21] F. Daniels, "Acoustical impedance of enclosures", Journal of the Acoustical Society of America **19**, 569–571 (1947).

[22] C. Zwikker and C. Kosten, *Sound Absorbing Materials*, 1–147 (Elsevier, New York) (1949).

[23] D. Keefe, "Acoustical wave propagation in cylindrical ducts: Transmission line parameter approximations for isothermal and nonisothermal boundary conditions", Journal of the Acoustical Society of America **75**, 58–62 (1984).

[24] R. Mignot and T. Hélie, "Acoustic modelling of a convex pipe adapted for digital waveguide simulation", in *Proceedings of the 13th International Digital Audio Effects Conference*, 95–101 (Graz, Austria) (2010).

[25] T. Hélie and D. Matignon, "Diffusive representations for the analysis and simulation of flared acoustic pipes with visco-thermal losses", Mathematical Models and Methods in Applied Sciences **16**, 503–536 (2006).

[26] T. Hélie, "Unidimensional models of acoustic propagation in axisymmetric waveguides", Journal of the Acoustical Society of America **114**, 2633–2647 (2003).

[27] H. Levine and J. Schwinger, "On the radiation of sound from an unflanged circular pipe", Physical Review **73**, 383–406 (1948).

[28] F. Silva, P. Guillemain, J. Kergomard, B. Mallaroni, and A. Norris, "Approximation forms for the acoustic radiation impedance of a cylindrical pipe", Journal of Sound and Vibration **322**, 255–263 (2009).

[29] L. Weinberg, *Network Analysis and Synthesis*, 1–692 (McGraw-Hill, New York, New York) (1962).

[30] T. Hélie and X. Rodet, "Radiation of a pulsating portion of a sphere: Application to horn radiation", Acta Acustica united with Acustica **89**, 565–577 (2003).

[31] J.-P. Dalmont, C. Nederveen, and N. Joly, "Radiation impedance of tubes withdifferent flanges: Numerical and experimental investigations", Journal of Sound and Vibration **244**, 505–534 (2001).

[32] M. Dablain, "The application of high-order differencing to the scalar wave equation", Geophysics **51**, 54–66 (1986).

[33] R. Leveque, *Finite Volume Methods for Hyperbolic Problems*, 1–578 (Cambridge University Press, Cambridge, UK) (2002).

[34] S. Bilbao, *Numerical Sound Synthesis: Finite Difference Schemes and Simulation in Musical Acoustics*, 256 (John Wiley and Sons, Chichester, UK) (2009).

[35] R. Courant, K. Friedrichs, and H. Lewy, "Über die partiellen Differenzengleichungen de mathematischen Physik", Mathematische Annalen **100**, 32–74 (1928).

[36] J. Kelly and C. Lochbaum, "Speech synthesis", in *Proceedings of the Fourth International Congress on Acoustics*, 1–4 (Copenhagen, Denmark) (1962), paper G42.

[37] Y. Chen and K. Moore, "Discretization schemes for fractional-order differentiators and integrators", IEEE Transactions on Circuits andSystems-I: Fundamental Theory and Applications **49**, 363–367 (2002).

[38] B. Vinagre, I. Podlubny, A. Hernandez, and V. Feliu, "Some approximationsof fractional order operators used in control theory and applications", Fractional Calculus and Applied Analysis **3**, 231–248 (2000).

[39] B. V. Y. Chen and I. Podlubny, "Continued fraction expansion approaches to discretizing fractional order derivatives-an expository review", Nonlinear Dynamics **38**, 155–170 (2012).

[40] A. Fettweis, "Wave digital filters: Theory and practice", Proceedings of the IEEE **74**, 270–327 (1986).

[41] A. Myers, "Characterization and taxonomy of historic brass musical instruments from an acoustical standpoint", Ph.D. thesis, University of Edinburgh (1998).

[42] S. Félix, J.-P. Dalmont, and C. Nederveen, "Effects of bending portions of the air column on the acoustical res-

onances of a wind instrument", Journal of the Acoustical Society of America **131**, 4164–4172 (2012).

[43] G. Widholm, H. Pichler, and T. Ossmann, "Bias: A computer-aided test system for brass wind instruments", Audio Engineering Society Paper (2834) (1989).

[44] G. Widholm, "Brass wind instrument quality measured and evaluated by a new computer system", in *Proceedings of the 15th International Congress on Acoustics*, volume III, 517–520 (Trondheim, Norway) (1995).

[45] A. Hirschberg, J. Gilbert, R. Msallam, and A. Wijnands, "Shock waves in trombones", Journal of the Acoustical Society of America **99**, 1754–1758 (1996).

[46] R. Msallam, S. Dequidt, S. Tassart, and R. Caussé, "Physical model of the trombone including nonlinear effects. Application to the sound synthesis of loud tones", Acta Acustica united with Acustica **86**, 725–736 (2000).

[47] C. Vergez and X. Rodet, "A new algorithm for nonlinear propagation of sound wave: Application to a physical model of a trumpet", Journal of Signal Processing **4**, 79–88 (2000).

[48] J. Gilbert, L. Menguy, and M. Campbell, "A simulation tool for brassiness studies", Journal of the Acoustical Society of America **123**, 1854–1857 (2008).

[49] C. Hirsch, *Numerical Computation of Internal and External Flows*, 1–538 (John Wiley and Sons, Chichester, UK) (1988).